Geophysical Research Letters

RESEARCH LETTER
10.1029/2023GL105983

Key Points:

- Sea surface salinity (SSS) in the central equatorial Pacific since ~1,780 ka was reconstructed by surface-dwelling foraminiferal $\delta^{18}O$ and Mg/Ca
- The reconstructed SSS shows a long-term freshening trend across the mid-Pleistocene transition
- The freshening trend primarily reflects the southward shift and intensification of the North Pacific intertropical convergence zone

Supporting Information:

Supporting Information may be found in the online version of this article.

Correspondence to:

X. Wang and Z. Jian,
xxwang@tongji.edu.cn;
jian@tongji.edu.cn

Citation:

Wang, X., Wang, Y., Dyez, K. A., Ravelo, A. C., Sun, C., Liu, F., et al. (2023). Southward shift and intensification of the intertropical convergence zone in the North Pacific across the mid-Pleistocene transition. *Geophysical Research Letters*, *50*, e2023GL105983. https://doi.org/10.1029/2023GL105983

Received 17 AUG 2023
Accepted 10 DEC 2023

Author Contributions:

Conceptualization: Xingxing Wang, Yue Wang, Zhimin Jian
Formal analysis: Xingxing Wang, Yue Wang, Kelsey A. Dyez
Funding acquisition: Xingxing Wang, Yue Wang, Zhimin Jian
Investigation: Xingxing Wang, Yue Wang, Kelsey A. Dyez
Methodology: Xingxing Wang, Kelsey A. Dyez, Chunxiao Sun, Xiaoying Jiang

© 2023. The Authors.
This is an open access article under the terms of the Creative Commons Attribution-NonCommercial-NoDerivs License, which permits use and distribution in any medium, provided the original work is properly cited, the use is non-commercial and no modifications or adaptations are made.

Southward Shift and Intensification of the Intertropical Convergence Zone in the North Pacific Across the Mid-Pleistocene Transition

Xingxing Wang[1], Yue Wang[1], Kelsey A. Dyez[2], A. Christina Ravelo[3], Chunxiao Sun[1], Fenghao Liu[1], Xiaoying Jiang[1], and Zhimin Jian[1]

[1]State Key Laboratory of Marine Geology, Tongji University, Shanghai, China, [2]Department of Earth and Environmental Sciences, University of Michigan, Ann Arbor, MI, USA, [3]Department of Ocean Sciences, University of California, Santa Cruz, CA, USA

Abstract The Hadley Circulation and associated westerlies strengthened and moved equatorward across the mid-Pleistocene transition (MPT). However, the evolution of the intertropical convergence zone (ITCZ) is still elusive due to the scarcity of long-term hydrological records from regions sensitive to the ITCZ change. Here, high-resolution sea surface salinity estimates derived from surface-dwelling planktic foraminiferal $\delta^{18}O$ and Mg/Ca in Ocean Drilling Program Site 871 reveal a long-term freshening trend in the central equatorial Pacific across the MPT. We attribute this secular reorganization of the precipitation-evaporation balance to the gradual southward migration and intensification of ITCZ in the North Pacific. It is inferred that the long-term evolution of the ITCZ was modulated by the increased meridional sea surface temperature gradients and the enhancements of trade winds across the MPT.

Plain Language Summary The Hadley circulation and westerlies have been revealed to strengthen and shift equatorward across the mid-Pleistocene transition (MPT), yet how the ITCZ, the uplifting branches of the Hadley Circulation, changed remains elusive. As precipitation is a key indicator of the ITCZ, here we use the residual oxygen isotope ($\delta^{18}O$) of calcite, calculated from planktic foraminiferal $\delta^{18}O$ and Mg/Ca, to reconstruct the sea surface salinity (SSS) change and track precipitation change in the central equatorial Pacific during the past ~1,780 kyr. In contrast to the stable SSS condition in the far western part of the Western Pacific, our new SSS record shows a striking secular decreasing trend across the MPT and represents a hydrological transition from evaporation-control to precipitation-control state. We suggest that the long-term hydrological reorganization was the result of the gradual southward migration and intensification of the North Pacific ITCZ across the MPT, which was closely related to the increased meridional sea surface temperature gradients and the enhancements of trade winds.

1. Introduction

The Earth's surface climate system underwent significant reorganizations since the mid-Pliocene. Especially across the mid-Pleistocene transition (MPT) period from ~1,250 ka to 700 ka, pronounced long-term cooling occurred in the mid-to high-latitudes and upwelling regions, leading to stronger meridional (poleward) and zonal (east-west) sea surface temperature (SST) gradients (Clark et al., 2006; Fedorov et al., 2015; McClymont et al., 2013). These SST gradients help to drive atmospheric and oceanic circulation, and thus the heat and moisture export from the tropical oceans (Brierley & Fedorov, 2010; Burls & Fedorov, 2017). Recently, several studies proposed that meridional and zonal circulation changes across the MPT played a critical role in heat and moisture transportation for promoting the Northern Hemisphere (NH) ice sheet growth (e.g., Barker et al., 2021; Catunda et al., 2021; de Garidel-Thoron et al., 2005; McClymont & Rosell-Melé, 2005), which highlights the coupling relationship between the tropical and extratropical regions.

As a main pathway of meridional heat and moisture transport, the atmospheric Hadley Circulation is composed of two parts: (a) surface trade winds cause moisture and latent heat to converge near the equator and form the intertropical convergence zone (ITCZ); (b) two upper tropospheric branches that diverge poleward from the ITCZ join the westerlies at mid-latitudes and transfer energy to the higher latitudes (Chiang & Friedman, 2012). The position and intensity of Hadley circulation, ITCZ and westerlies are greatly modulated by inter- or inner-hemispheric heating gradients (Schneider et al., 2014). Previous studies suggest that the ITCZ will not

Project Administration: Xingxing Wang, Yue Wang, Zhimin Jian
Resources: Kelsey A. Dyez, A. Christina Ravelo, Zhimin Jian
Software: Xingxing Wang, Fenghao Liu
Supervision: Zhimin Jian
Validation: Xingxing Wang
Writing – original draft: Xingxing Wang, Yue Wang, Zhimin Jian
Writing – review & editing: Xingxing Wang, Yue Wang, Kelsey A. Dyez, A. Christina Ravelo, Zhimin Jian

only migrate to a relatively warmer hemisphere but also can contract/expand in the latitudinal range to modulate monsoonal rainfall changes on orbital-to millennial-scales (e.g., Broccoli et al., 2006; Chiang & Bitz, 2005; Sachs et al., 2009; Schmidt & Spero, 2011; Yan et al., 2015; Zhang et al., 2022). However, less is known about the long-term evolution of the ITCZ mean position and intensity, and its relation to the meridional SST gradient in the Quaternary.

Following the gradual growth of the NH ice sheet, the Hadley Circulation has grown stronger since the Pliocene (Brierley et al., 2009; Etourneau et al., 2010; Fedorov et al., 2015; Jia et al., 2008) while associated westerlies have intensified and moved equatorward (Abell et al., 2021; Taylor et al., 2022; Zhong et al., 2022). Yet for the ITCZ, large uncertainties lie not only in the influence of the NH ice sheet but also in the influence of the western Pacific warm pool (WPWP) which modulates three-dimensional seawater temperature gradients in the Pacific. For example, before the MPT, the WPWP may have been at a more northerly position and with more asymmetry about the equator (Jia et al., 2008; Russon et al., 2010), which may favor a northward ITCZ. After the MPT, increased dust input from the Asian continent to the central equatorial Pacific (CEP) indicates a southward shift of ITCZ (Seo et al., 2015). Generally, precipitation is also considered as powerful evidence of ITCZ position, but most hydrological paleo-records from the far western part of WPWP show stable sea surface salinity (SSS) across the MPT (de Garidel-Thoron et al., 2005; Medina-Elizalde & Lea, 2005), probably because the rainband in this region is less sensitive to ITCZ displacement than the central and eastern Pacific (Atwood et al., 2020). Thus, reliable hydrological records with high temporal resolution from the CEP will be essential to reveal ITCZ positioning across the MPT.

Here we present a new ~1,780 kyrs' stable oxygen isotope ($\delta^{18}O$) record of surface-dwelling planktic foraminifera *Globigerinoides ruber* in the CEP, extend the previously published 1,400 kyrs' Mg/Ca-SST record in this site to 1,780 ka, and calculate residual $\delta^{18}O$ of seawater to track SSS change. We further compare the SST and SSS records in the tropical Pacific to illustrate the unique thermal and hydrological changes in the CEP. Finally, we compare our records with meridional SST gradients to discuss the influence of atmospheric circulation on the hydrological changes in the CEP.

2. Materials and Methods

The samples used in this study were collected from Ocean Drilling Program Site 871 (ODP871), located at 5°33′N, 172°21′E at a water depth of 1,255 m (Figure 1), atop the drowned platform of Limalok Guyot in the Ratak Chain of the Southern Marshall Islands (Shipboard Scientific Party, 1993). The top 26.5 m unit of ODP871 is composed of light gray nannofossil foraminifer ooze at ~1 cm/kyr sedimentation rate containing the whole Pleistocene (Shipboard Scientific Party, 1993). The sampling rate is 1 sample every 3 cm (~3 kyr).

Previous studies have published a portion of the *G. ruber* Mg/Ca record (past 1,400 ka) (Dyez & Ravelo, 2013, 2014). In this study, new *G. ruber* Mg/Ca data are presented to extend the record to 1,780 ka. For each sample, 40–60 *G. ruber* (white) specimens were picked from the 250–355 μm size fraction and then crushed and split into two portions to be analyzed for isotopic and elemental ratios. After the same cleaning procedures as in previous studies, established by Boyle and Keigwin (1985), new *G. ruber* Mg/Ca ratios were measured by inductively coupled plasma optical emission spectrometry at the University of California Santa Cruz (UCSC) with 1σ standard deviation of 0.21 mmol/mol, or ~0.5°C, based on repeated measurements of internal foraminifer reference standards (Dyez & Ravelo, 2014). Here SST was calculated from the *G. ruber* Mg/Ca ratio using the Mg/Ca-SST equations ($Mg/Ca = 0.26\ (\pm 0.04)\ \exp(0.097\ (\pm 0.006) \times SST)$) established for the WPWP (Hollstein et al., 2017). The same approach is applied to other reference sites by adjusting exponential coefficients and pre-exponents to match their modern observed SST values (Table 1).

For $\delta^{18}O$ analysis, the crushed *G. ruber* shells were ultrasonically rinsed in methanol. *G. ruber* $\delta^{18}O$ of samples from 0 to 290 ka were measured by a Fisons PRISM mass spectrometer at UCSC with a standard deviation (1σ) of 0.05‰. Additional *G. ruber* $\delta^{18}O$ samples from 290 to 1,780 ka were analyzed at the State Key Laboratory of Marine Geology, Tongji University, using a Finnigan-MAT253 mass spectrometer, with a standard deviation better than 0.07‰. The oxygen isotope results were calibrated to the international Pee Dee Belemnite scale by international standards NBS18 and NBS19. Even though small portions of the $\delta^{18}O$ record were generated in two different labs (Tongji and UCSC), there is no significant interlaboratory offset and the changes through the MPT are not driven by interlaboratory differences.

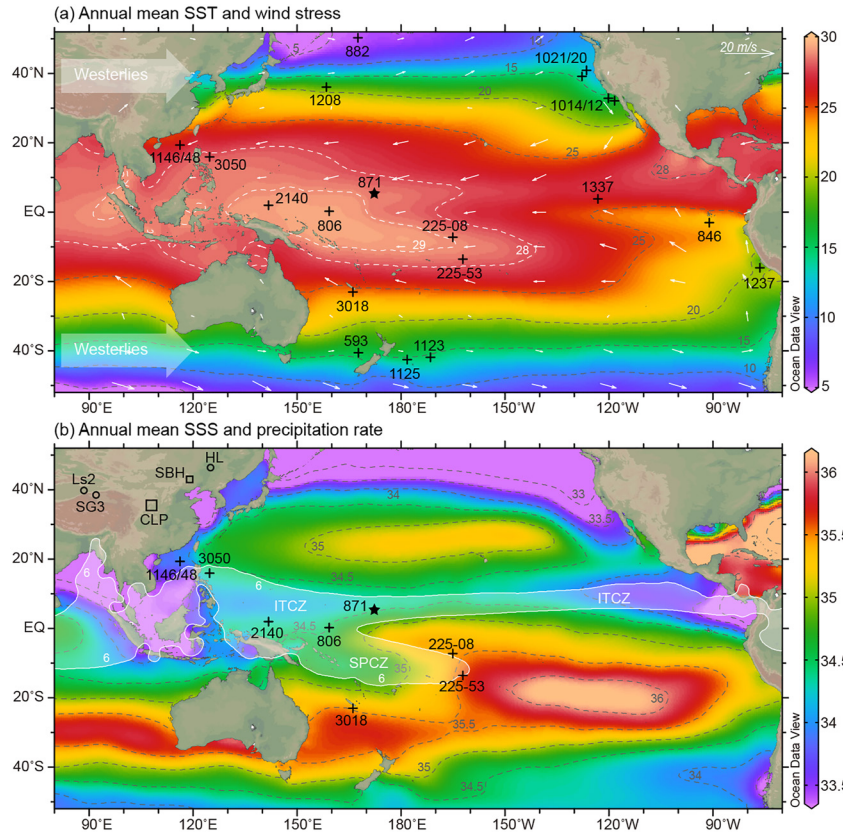


Figure 1. (a) Annual mean sea surface temperature (color shaded) distributions in the Pacific derived from WOA13 (Locarnini et al., 2013), in which white dashed lines represent the western Pacific warm pool (28°C; Yan et al., 1992) and its heart region (29°C). White arrows indicate annual mean wind stress based on NCEP/NCAR reanalysis data (Kalnay et al., 1996), and white filled arrows indicate the westerlies at mid-latitudes. (b) Annual mean sea surface salinity (color shaded) in the Pacific derived from WOA13 (Zweng et al., 2013). The distributions of intertropical convergence zone and south Pacific convergence zone are indicated by the white shading areas with annual mean precipitation rate of more than 6 mm day^{-1} based on CAMP precipitation data (https://psl.noaa.gov/data/gridded/data.cmap.html). The black stars indicate site ODP871 of this study and other black markers of crosses, empty circles and squares are reference sites. The maps are created using Ocean Data View (Schlitzer, 2015).

The $\delta^{18}O$ of foraminifera carbonate ($\delta^{18}O_c$) is a result of both the calcification temperature and seawater $\delta^{18}O$ ($\delta^{18}O_{sw}$); variations of $\delta^{18}O_{sw}$ are typically controlled by changes in global ice volume, advection and precipitation-evaporation, which are related to local salinity. Thus, after subtracting the contributions of ice volume ($\delta^{18}O_{ice}$) and calcification temperature, the residual proportion ($\delta^{18}O_{re}$) of *G. ruber* $\delta^{18}O$ can be used to reconstruct local salinity changes (e.g., Mohtadi et al., 2014; Schmidt & Spero, 2011). Due to the relatively constant $\delta^{18}O_{re}$-salinity relationship across spatial and temporal scales, paleo-salinity reconstructions in the

Table 1
Information of Reference Sites in the Western Pacific Warm Pool

Core	Longitude	Latitude	Water depth (m)	Time resolution (kyr)	Species	*A*	*B*	*a*
ODP871	172.34	5.56	1,255	~3	*G. ruber*	0.097	0.26	16.5
ODP806	159.35	0.36	2,520	~2.5	*G. ruber*	0.097	0.23	16.5
MD2140	141.77	2.03	2,547	~5	*G. ruber*	0.097	0.27	16.5
SO225-08	−165.05	−7.20	2,589	~10	*T. sacculifer*	0.097	0.26	14.9
SO225-53	−162.14	−13.52	3,150	~8	*T. sacculifer*	0.097	0.25	14.9
MD3018	166.15	−23.00	2,470	~5	*G. ruber*	0.101	0.31	14.9

Note. *A* and *B* are the coefficients of the SST equations. *a* is the constant in the $\delta^{18}O_{sw}$ equation.

tropical Pacific are thought to be reliable (Holloway et al., 2016). Here $\delta^{18}O_{sw}$ was calculated using the $\delta^{18}O_{sw}$-temperature relationship given by Bemis et al. (1998), $\delta^{18}O_{sw} = [T\ (°C) - a + 4.8 \times \delta^{18}O_c]/4.8 + 0.27$, where $\delta^{18}O_c$ and T represent *G. ruber* $\delta^{18}O$ and SST, respectively, and the constant a is adjusted to match modern values (Table 1). $\delta^{18}O_{ice}$ was based on the simulated data from Bintanja and van de Wal (2008). Following the method of Mohtadi et al. (2014), the average error in $\delta^{18}O_{re}$ is estimated as ±0.16‰, based on the errors of $\delta^{18}O_c$ (±0.07‰), $\delta^{18}O_{ice}$ (±0.09‰; Bintanja & van de Wal, 2008) and SST (±0.5°C; Dyez & Ravelo, 2014). SSS was calculated from $\delta^{18}O_{re}$ using the Holocene relationship in the western tropical Pacific (LeGrande & Schmidt, 2011): $\delta^{18}O_{re} = 0.65 \times SSS - 21.52$. All the $\delta^{18}O_{re}$ (SSS) records used in this study were corrected for sea level change in the same way as ODP871.

The previously published age model of ODP871 over the past 1,400 ka was established by $\delta^{18}O$ records of *Uvigerina* spp. (Dyez & Ravelo, 2013, 2014). Here, we extended the *Uvigerina* $\delta^{18}O$ record from 1,400 ka to 1,780 ka with an extra 120 samples. For each sample, ~3 specimens of *Uvigerina* spp. (>250 μm) were picked, crushed, rinsed in methanol and measured at the State Key Laboratory of Marine Geology, Tongji University. The new age model for ODP871 (Figure S1 in Supporting Information S1) is updated here by aligning the *Uvigernia* $\delta^{18}O$ record with the LR04 $\delta^{18}O$ stack (Lisiecki & Raymo, 2005) using QAnalySeries matching software (Kotov & Pälike, 2018).

3. Results and Discussion

3.1. Cooling and Freshening Trend in the Northeastern WPWP

The new SST record of ODP871 shows clear glacial-interglacial cycles during the ~1,780–1,400 ka, with smaller amplitudes than in the late Pleistocene (Figure 2b). Previous reconstructions demonstrated that SSTs in the central WPWP were stable throughout the Pleistocene epoch, displaying no discernible long-term trend (de Garidel-Thoron et al., 2005; McClymont & Rosell-Melé, 2005; Medina-Elizalde & Lea, 2005). However, the SST record of ODP871, which is located at the northeastern margin of the WPWP, displays a slight cooling trend (~1.1°C) during ~1,400–1500 ka. The slight long-term cooling trend is consistent with global gradual cooling, which occurred both during glacials and interglacials (Figure 2 and Figure S2 in Supporting Information S1).

SST distributions are strongly affected by sea surface wind stress and land distributions. The isotherms of modern annual mean SST present southwestward and westward concave shapes in the northeastern and eastern WPWP, respectively (Figure 1a). This implies that SSTs in the northeastern WPWP are sensitive to northeast trade winds while SSTs in the eastern WPWP are sensitive to equatorial easterlies. As global long-term cooling across the MPT, the northern boundary of the WPWP shifted equatorward as indicated by the cooling trend of SST on the northern margin of the warm pool (Herbert et al., 2010; Jia et al., 2008), in contrast to the relatively stable SST patterns near the southern margin (Raddatz et al., 2017; Russon et al., 2010). Meanwhile, sea surface cooling was also recorded in the northeastern Pacific (NEP; Brierley et al., 2009; Dekens et al., 2007; LaRiviere et al., 2012; Liu et al., 2008), which increased the SST gradient between the WPWP and the northeastern Pacific and thus enhanced the northeast trade winds. We infer that the long-term cooling trend and the southwestward shifted boundary in the northeastern WPWP are very related to the progressive strengthening of trade winds through the MPT. Along with the development of cold tongue in the eastern equatorial Pacific (EEP) (Herbert et al., 2010), the existing SST reconstructions imply that the WPWP was gradually displaced southward with its northern and eastern margins moved centerward across the MPT.

Most planktic foraminiferal $\delta^{18}O$ records in the WPWP varied nearly in concert with SST records throughout the Pleistocene (Figure 2), for example, those $\delta^{18}O$ records in the central and southern WPWP all remain stable (de Garidel-Thoron et al., 2005; Medina-Elizalde & Lea, 2005; Raddatz et al., 2017; Russon et al., 2011; Wara et al., 2005). *G. ruber* $\delta^{18}O$ records in the northern margin of WPWP (ODP1146 and MD3050) gradually increased across the MPT (Clemens & Prell, 2003; Sun et al., 2017), which could reflect the influence of local SST cooling. However, *G. ruber* $\delta^{18}O$ record of ODP871 shows the opposite; a striking long-term decreasing trend (~1‰) during ~1,600–1500 ka, in contrast with local sea surface gradual cooling (Figure 2).

Although similar trends exist in planktic foraminiferal $\delta^{18}O$ records in the central and southeastern WPWP, there is a big gap between their mean values (i.e., −1.8‰ at MD2140 and −0.8‰ at SO225) (de Garidel-Thoron et al., 2005; Raddatz et al., 2017). *G. ruber* $\delta^{18}O$ results of ODP871 are consistent with SO225 before ~1,600 ka while close to MD2140 since ~500 ka. Modern sea surface $\delta^{18}O_{sw}$ can be used to indicate the SSS changes (LeGrande & Schmidt, 2011). In the far western part of WPWP (e.g., MD2140), salinity is relatively fresh (SSS <34.5 psu) (Zweng et al., 2013) and is primarily controlled by deep convection (precipitation rate >8 mm/day). In the southeastern WPWP (e.g., SO225), salinity is relatively higher (~35.5 psu) (Zweng et al., 2013) and is

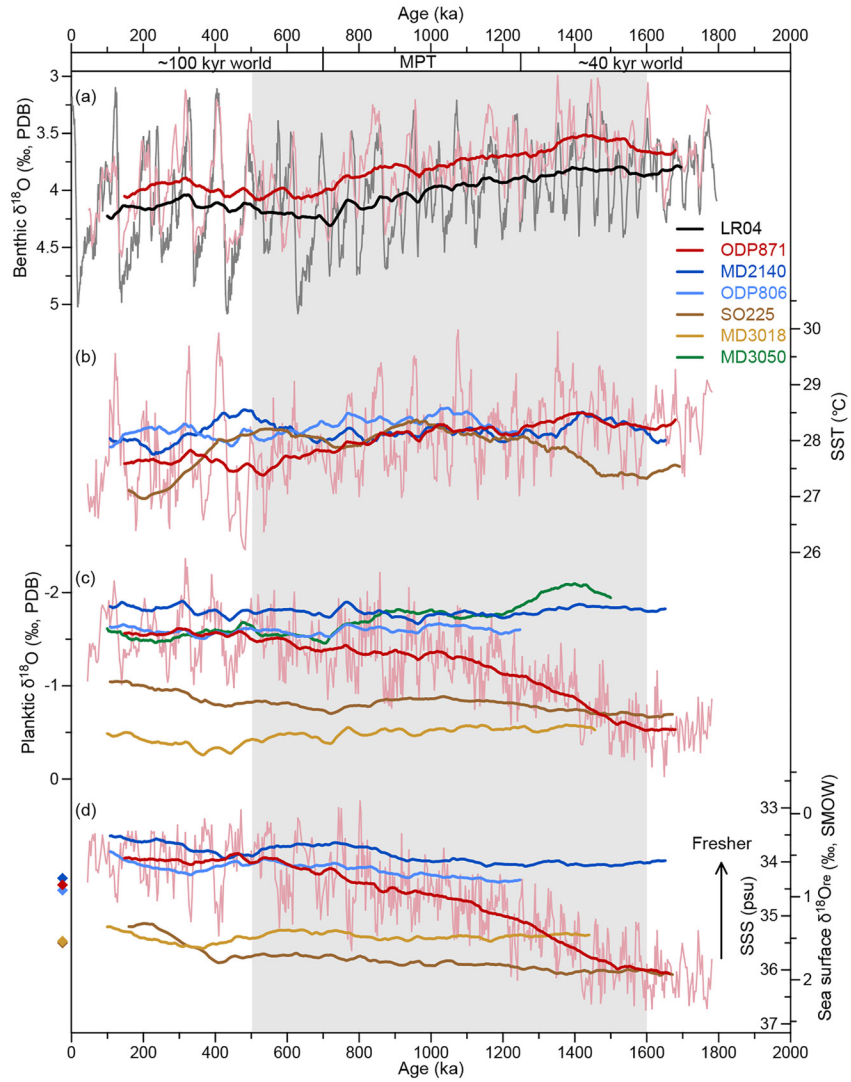


Figure 2. Proxy records in the western Pacific. (a) LR04 $\delta^{18}O$ stack (Lisiecki & Raymo, 2005) and 3-point running average of ODP871 *Uvigerina* spp. $\delta^{18}O$ (Dyez & Ravelo, 2013, 2014; this study); (b) sea surface temperature, (c) planktic $\delta^{18}O$, and (d) sea surface $\delta^{18}O_{re}$ and corresponding sea surface salinity (SSS) records: MD2140 (de Garidel-Thoron et al., 2005), ODP806 (Medina-Elizalde & Lea, 2005), ODP871 (Dyez & Ravelo, 2013, 2014; this study), SO225-05 and SO225-53 (SO225; Raddatz et al., 2017), MD3018 (Russon et al., 2010, 2011), MD3050 (Sun et al., 2017). The thick line represents a 200 kyr running average, calculated from a constant 4 kyr resolution record interpolated from the original record. The diamonds indicate the modern annual mean SSS values of reference sites based on WOA13 data (Zweng et al., 2013). The gray bar indicates the interval with the long-term changes of *G. ruber* $\delta^{18}O$ and SSS records at ODP871.

controlled by intense evaporation. *G. ruber* $\delta^{18}O$ and $\delta^{18}O_{re}$ (SSS) records in the central and southeastern WPWP exactly reflect the salinity difference between these two regions (Figure 2). Between these two end members, the striking secular decreasing trend of *G. ruber* $\delta^{18}O_{re}$ in ODP871 suggests that its long-term mean SSS substantially decreased from ~36 psu before 1,600 ka to ~34 psu after 500 ka (Figure 2d and Figure S3 in Supporting Information S1). This drastic hydrological reorganization may indicate that the northeastern WPWP transitioned from an evaporation-control state to a precipitation-control state across the MPT, as detailed below.

3.2. Mechanism for Hydrological Changes in the Northeastern WPWP

The modern SSS changes are highly correlated to precipitation variations at Site ODP871 (Figure S4 in Supporting Information S1). Hydrological variations in the WPWP are primarily regulated by zonal Walker Circulation and meridional Hadley Circulation, which are closely related to El Niño-Southern Oscillation (ENSO) and ITCZ,

respectively (Schmidt & Spero, 2011; Stott et al., 2002). During modern La Niña stages, strong Walker Circulation confines deep convection to the far western part of WPWP, bringing intensive precipitation to the Maritime Continent. While under El Niño stages, weak Walker Circulation facilitates eastern displacement of the deep convection center to increase precipitation in the CEP (Dai & Wigley, 2000). ODP871 is located at the northeastern margin of the WPWP, closer to the CEP. Modern observation demonstrates the El Niño state promotes much fresher conditions in the ODP871 area than in MD2140 while similar conditions under the La Niña state (Carton & Giese, 2008; Figure S5 in Supporting Information S1).

Paleo-temperature reconstructions revealed that during the Pliocene warm period, the equatorial Pacific was under a permanent El Niño-like condition with a smaller zonal SST gradient, less of a difference in thermocline depth and weaker Walker Circulation (Ford et al., 2015; Wara et al., 2005). Then the zonal SST gradient gradually became pronounced since ∼1,700 ka and reached modern values by ∼900 ka, extensively enhancing the Walker Circulation (de Garidel-Thoron et al., 2005; Fedorov et al., 2015; McClymont & Rosell-Melé, 2005; Wara et al., 2005). Persistent intensification of chemical weathering in Papua New Guinea also corroborates a strengthening of Walker Circulation over the past ∼1,700 ka (Peng et al., 2021). However, the steady enhancement of Walker Circulation across the MPT should induce gradually saltier sea surface conditions in the CEP, which is contrary to the progressive freshening trend observed in ODP871. This leaves the ITCZ changes as a more plausible explanation for the freshening at ODP871.

In the central Pacific region east of 170°E, the ITCZ migrates between 2°N and 9°N with minimal seasonal changes (Schneider et al., 2014), and the ITCZ rainband is highly tied to a narrow low-SSS zone (Figure 1b). Paleoclimatic simulations indicated that a smaller meridional SST gradient during the Pliocene weakened the NH Hadley Circulation, with a northward center and larger latitudinal extent, which moved the ITCZ northward and widened its latitudinal range and reduced its convection and precipitation intensity (Brierley et al., 2009; Burls & Fedorov, 2017; Pontes et al., 2022). Thus, the long-term freshening trend of ODP871 could be caused by increased precipitation due to the southward shift and intensification of the Pacific ITCZ, and/or by the increased advection of low-salinity surface water from the northeastern Pacific, which are all regulated by increased meridional SST gradients and associated intensification of Hadley Circulation and trade winds.

Model simulations revealed that the meridional shifts of ITCZ mean position are dynamically modulated by the Hadley Circulation, trade winds and cross-equatorial temperature gradient (Broccoli et al., 2006; Chiang & Bitz, 2005; McGee et al., 2018; Schneider et al., 2014). In these models, the increased meridional SST gradient drives an enhanced Hadley Circulation, involving processes of mid-latitudes cooling, energetic trade winds, and southward displacements of westerlies and ITCZ. Across the MPT, a more significant secular cooling trend occurred in the NH mid-latitudes than in the Southern Hemisphere (Figure 3a), accompanied by a gradual negative north-to-south cross-equatorial SST gradient (Figure 3c). In addition, the SSTs in the northeastern Pacific decreased (Brierley et al., 2009; Dekens et al., 2007; LaRiviere et al., 2012; Liu et al., 2008) to enlarge the SST gradient between the WPWP and northeastern Pacific and intensify the northeast trade winds (Figure 3b). Meanwhile, NH westerlies were also strengthened and moved equatorward across the MPT (Taylor et al., 2022; Zhong et al., 2022). All the above dynamical aspects support the southward shift of the ITCZ mean position. Model simulations suggest that the mean position shifts of the ITCZ are generally less than 1° latitude in magnitude (Donohoe et al., 2022; McGee et al., 2014), but due to changes in atmospheric dynamics, the meridional shift range and intensity of the ITCZ vary highly correlated and can be used to explain major fractions of tropical precipitation changes (Donohoe et al., 2022). Note that precipitation in the ITCZ is driven by moisture convergence associated with the northerly and southerly trade winds that collide near the equator, induced by meridional SST gradients (Byrne et al., 2018). Across the MPT, the SST gradient between the EEP and southeastern Pacific (SEP) also increased as the SEP cooled significantly (Dekens et al., 2007) to strengthen the southeast trade winds (Figure 3b). Thus, the strengthening trade winds in both hemispheres are conducive to the atmosphere's convergence and uplift, thus narrowing the meridional shift range of the ITCZ and intensifying the precipitation. However, as the NH cooled in a larger amplitude, the northern margin of the WPWP displaced southward and decreased north-to-south cross-equatorial SST gradient (Figure 3c), we suggest that the northern margin of the ITCZ latitudinal extent gradually southward displaced to generate the southward movement of ITCZ mean position, which synchronously contributed to reduce the ITCZ latitudinal extent to bring more rainfall to the CEP.

4. Conclusions and Implications

In comparison to the long-term stable SST in the central WPWP, ODP871 SST gradually cooled across the MPT, which may be related to the enhancement of the northeast trade winds. Moreover, unlike the less dramatic

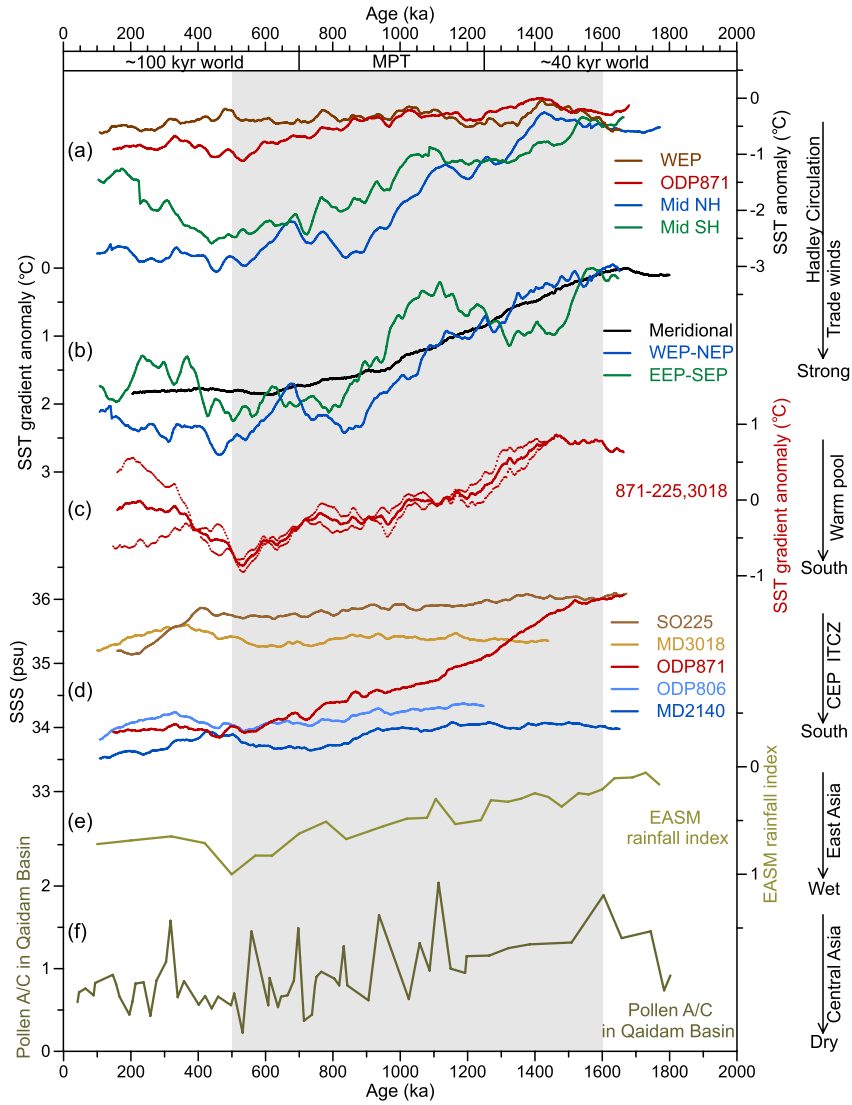


Figure 3. Comparison of proxy records of sea surface temperature (SST) gradients and sea surface salinity (SSS). (a) SST anomalies of the western equatorial Pacific (WEP) (MD2140, ODP806; de Garidel-Thoron et al., 2005; Medina-Elizalde & Lea, 2005), ODP871 (Dyez & Ravelo, 2013, 2014; this study), mid-NH (ODP1208, ODP1020, ODP1021, ODP1014, ODP1012; Brierley et al., 2009; Dekens et al., 2007; LaRiviere et al., 2012; Liu et al., 2008) and mid-SH (DSDP593, ODP1125, ODP1123, ODP1237; Crundwell et al., 2008; Dekens et al., 2007; McClymont et al., 2016; Peterson et al., 2020); (b) meridional SST gradient anomaly (Fedorov et al., 2015) and SST gradient anomaly between the WEP and northeast Pacific (NEP, ODP1020, ODP1021, ODP1012, ODP1014), and SST gradient anomaly between the eastern equatorial Pacific (EEP, U1337 and ODP846; Herbert et al., 2010; Liu et al., 2019) and southeast Pacific (southeastern Pacific, ODP1237; Dekens et al., 2007); (c) SST gradient anomalies between northern and southern margin of WPWP; (d) SSS records in the WPWP; (e) East Asian summer monsoon rainfall index in the Chinese Loess Plateau (Meng et al., 2018); (f) pollen A/C in Qaidam Basin (Cai et al., 2012). The SST anomaly is calculated from the 200 kyr running average subtracting the maximum value over the whole-time window. The gray bar indicates the interval with the long-term change of SSS record at ODP871.

changes in *G. ruber* $\delta^{18}O$ of other western Pacific cores since the early Pleistocene, our high-resolution *G. ruber* $\delta^{18}O$ record of ODP871 exhibits a long-term decreasing trend during the period ~1,600–1500 ka. As SST cooling generally increases calcite $\delta^{18}O$, the decreasing *G. ruber* $\delta^{18}O$ suggests a prominent decrease in SSS, implying that the northeastern WPWP hydrology transitioned from an evaporation-dominated state to a precipitation-dominated state across the MPT. As strengthening Walker Circulation across the MPT would typically induce a rainfall decline in the CEP, we suggest that the intensification of the Walker Circulation is not the driver of our SSS change. Instead, we suggest that the decreasing SSS trend reflects the increased precipitation due to the southward shift and intensification of ITCZ in the North Pacific, and/or the increased advection of

low-salinity surface water from the northeastern Pacific, which were modulated by the increased meridional SST gradients and related enhancement of the trade winds.

The MPT (~1,250–1700 ka) primarily represents the span time of the glacial-interglacial cycle changed from ~41 to ~100 kyr, but the expansion of NH ice-sheet started earlier and persisted longer indicated by increased magnetic susceptibility of Site ODP882 (Haug et al., 1999; Figure S6b in Supporting Information S1). This earlier and persisted cooling of NH extratropics was also accompanied by increased meridional SST gradient and intensification of Hadley Circulation (Fedorov et al., 2015), and finally a southward shift and intensification of the central Pacific ITCZ variation indicated by the freshening trend of Site ODP871 (~1,600–500 ka). While many studies suggested that the intensification of meridional oceanic circulation in the Atlantic (Bahr et al., 2018; Barker et al., 2021; Catunda et al., 2021) and Pacific (Taylor et al., 2022) could deliver more moisture to the high latitudes and promote for the NH ice-sheet growth, the influence of atmospheric moisture and energy transport should not be neglected.

As shown above, the nearly consistent duration between the long-term southward shift and intensification of ITCZ and the gradual growth of the NH ice-sheet highlights the coupling relationship between tropical and extratropical regions. Previously, de Garidel-Thoron et al. (2005) and McClymont and Rosell-Melé (2005) proposed that Walker Circulation changes across the MPT might alter the meridional heat and moisture transfer to the NH high latitudes. Recent model simulations suggested that changes in the ITCZ position could impact the ENSO variability (Pontes et al., 2022), which may further complicate the influence of Walker Circulation changes. Although we can not fully rule out the impact of ENSO, it seems unlikely to explain the long-term freshening in our proxy merely using modern ENSO-like dynamics as an analogue. Thus we argue that meridional ITCZ dynamics may be a more reasonable explanation for our central Pacific record, and may represent an additional potential feedback on NH ice-sheet expansion besides the ocean circulation.

Furthermore, the ITCZ and associated Hadley circulation changes play a crucial role in regulating hydroclimate variations in mid-to-low latitudes (Burls & Fedorov, 2017; Chiang & Friedman, 2012; Jia et al., 2008; Zhao et al., 2020). Hydrological reconstructions from different regions present inconsistent long-term evolution of the East Asian summer monsoon (EASM) across the MPT. For example, many paleo-monsoon proxies suggest progressive aridification in northern China across the MPT (Cai et al., 2012; Liu et al., 2020; Zeng et al., 2020; Zhan et al., 2023; Figure 3f), while there is a prominent secular increasing rainfall trend in the carbonate $\delta^{13}C$ based EASM rainfall index from the Chinese Loess Plateau (Figure 3e), suggesting a gradual strengthening EASM (Meng et al., 2018). Across the MPT, the intensified and equatorward moved Hadley Circulation may drive the EASM rainfall to decrease in northern China but increase in middle-southeastern China, which is similar to the regional heterogenous rainfall variability regulated by Hadley Circulation on the interannual (Chiang et al., 2017) and orbital (Zhao et al., 2020) scales. Therefore, the southward shift and intensification of the ITCZ together with the westerlies can facilitate the intensification and southward shift of the Hadley Circulation, and hence enhance paleo-monsoons on a long-term time scale.

Data Availability Statement

New Mg/Ca and $\delta^{18}O$ data will be uploaded to the National Centers for Environmental Information: https://www.ncei.noaa.gov/access/paleo-search/. The data reported here are also stored in the Zenodo database (Wang et al., 2023).

Acknowledgments
We are grateful to the Integrated Ocean Drilling Program for providing samples. Financial supports for this study were from the National Natural Science Foundation of China (Grant 42106060, 41976047 and 91958208) and the State Key Laboratory of Marine Geology, Tongji University (Grant MG202101). Yue Wang is also sponsored by Shanghai Pilot Program for Basic Research. Two anonymous reviewers are also acknowledged for the constructive comments.

References

Abell, J. T., Winckler, G., Anderson, R. F., & Herbert, T. D. (2021). Poleward and weakened westerlies during Pliocene warmth. *Nature*, *589*(7840), 70–75. https://doi.org/10.1038/s41586-020-03062-1

Atwood, A. R., Donohoe, A., Battisti, D. S., Liu, X., & Pausata, F. S. R. (2020). Robust longitudinally variable responses of the ITCZ to a Myriad of climate forcings. *Geophysical Research Letters*, *47*(17), e2020GL088833. https://doi.org/10.1029/2020gl088833

Bahr, A., Kaboth, S., Hodell, D., Zeeden, C., Fiebig, J., & Friedrich, O. (2018). Oceanic heat pulses fueling moisture transport towards continental Europe across the mid-Pleistocene transition. *Quaternary Science Reviews*, *179*, 48–58. https://doi.org/10.1016/j.quascirev.2017.11.009

Barker, S., Zhang, X., Jonkers, L., Lordsmith, S., Conn, S., & Knorr, G. (2021). Strengthening Atlantic inflow across the mid-Pleistocene transition. *Paleoceanography and Paleoclimatology*, *36*(4), e2020PA004200. https://doi.org/10.1029/2020pa004200

Bemis, B. E., Spero, H. J., Bijma, J., & Lea, D. W. (1998). Reevaluation of the oxygen isotopic composition of planktonic foraminifera: Experimental results and revised paleotemperature equations. *Paleoceanography*, *13*(2), 150–160. https://doi.org/10.1029/98pa00070

Bintanja, R., & van de Wal, R. S. (2008). North American ice-sheet dynamics and the onset of 100,000-year glacial cycles. *Nature*, *454*(7206), 869–872. https://doi.org/10.1038/nature07158

Boyle, E. A., & Keigwin, L. D. (1985). Comparison of Atlantic and Pacific paleochemical records for the last 215,000 years: Changes in deep ocean circulation and chemical inventories. *Earth and Planetary Science Letters*, *76*(1–2), 135–150. https://doi.org/10.1016/0012-821X(85)90154-2

Brierley, C. M., & Fedorov, A. V. (2010). Relative importance of meridional and zonal sea surface temperature gradients for the onset of the ice ages and Pliocene-Pleistocene climate evolution. *Paleoceanography*, *25*(2), PA2214. https://doi.org/10.1029/2009pa001809

Brierley, C. M., Fedorov, A. V., Liu, Z., Herbert, T. D., Lawrence, K. T., & Lariviere, J. P. (2009). Greatly expanded tropical warm pool and weakened Hadley circulation in the early Pliocene. *Science*, *323*(5922), 1714–1718. https://doi.org/10.1126/science.1167625

Broccoli, A. J., Dahl, K. A., & Stouffer, R. J. (2006). Response of the ITCZ to Northern Hemisphere cooling. *Geophysical Research Letters*, *33*(1), L01702. https://doi.org/10.1029/2005gl024546

Burls, N. J., & Fedorov, A. V. (2017). Wetter subtropics in a warmer world: Contrasting past and future hydrological cycles. *Proceedings of the National Academy of Sciences of the United States of America*, *114*(49), 12888–12893. https://doi.org/10.1073/pnas.1703421114

Byrne, M. P., Pendergrass, A. G., Rapp, A. D., & Wodzicki, K. R. (2018). Response of the intertropical convergence zone to climate change: Location, width, and strength. *Current Climate Change Reports*, *4*, 355–370. https://doi.org/10.1007/s40641-018-0110-5

Cai, M., Fang, X., Wu, F., Miao, Y., & Appel, E. (2012). Pliocene–Pleistocene stepwise drying of Central Asia: Evidence from paleomagnetism and sporopollen record of the deep borehole SG-3 in the western Qaidam Basin, NE Tibetan Plateau. *Global and Planetary Change*, *94–95*, 72–81. https://doi.org/10.1016/j.gloplacha.2012.07.002

Carton, J. A., & Giese, B. S. (2008). A reanalysis of ocean climate using simple ocean data assimilation (SODA). *Monthly Weather Review*, *136*(8), 2999–3017. https://doi.org/10.1175/2007mwr1978.1

Catunda, M. C. A., Bahr, A., Kaboth-Bahr, S., Zhang, X., Foukal, N. P., & Friedrich, O. (2021). Subsurface heat channel drove Sea Surface warming in the high-latitude north Atlantic during the mid-Pleistocene transition. *Geophysical Research Letters*, *48*(11), e2020GL091899. https://doi.org/10.1029/2020gl091899

Chiang, J. C. H., & Bitz, C. M. (2005). Influence of high latitude ice cover on the marine Intertropical Convergence Zone. *Climate Dynamics*, *25*(5), 477–496. https://doi.org/10.1007/s00382-005-0040-5

Chiang, J. C. H., & Friedman, A. R. (2012). Extratropical cooling, interhemispheric thermal gradients, and tropical climate change. *Annual Review of Earth and Planetary Sciences*, *40*(1), 383–412. https://doi.org/10.1146/annurev-earth-042711-105545

Chiang, J. C. H., Swenson, L. M., & Kong, W. (2017). Role of seasonal transitions and the westerlies in the interannual variability of the East Asian summer monsoon precipitation. *Geophysical Research Letters*, *44*(8), 3788–3795. https://doi.org/10.1002/2017gl072739

Clark, P. U., Archer, D., Pollard, D., Blum, J. D., Rial, J. A., Brovkin, V., et al. (2006). The middle Pleistocene transition: Characteristics, mechanisms, and implications for long-term changes in atmospheric pCO2. *Quaternary Science Reviews*, *25*(23–24), 3150–3184. https://doi.org/10.1016/j.quascirev.2006.07.008

Clemens, S. C., & Prell, W. L. (2003). Data report: Oxygen and carbon isotopes from Site 1146, northern South China Sea. In W. L. Prell, P. Wang, P. Blum, D. K. Rea, & S. C. Clemens (Eds.), *Proceedings of the ocean Drilling Program* (Vol. 184, pp. 1–8). Scientific Results.

Crundwell, M., Scott, G., Naish, T., & Carter, L. (2008). Glacial–interglacial ocean climate variability from planktonic foraminifera during the Mid-Pleistocene transition in the temperate Southwest Pacific, ODP Site 1123. *Palaeogeography, Palaeoclimatology, Palaeoecology*, *260*(1–2), 202–229. https://doi.org/10.1016/j.palaeo.2007.08.023

Dai, A., & Wigley, T. M. L. (2000). Global patterns of ENSO-induced precipitation. *Geophysical Research Letters*, *27*(9), 1283–1286. https://doi.org/10.1029/1999gl011140

de Garidel-Thoron, T., Rosenthal, Y., Bassinot, F., & Beaufort, L. (2005). Stable sea surface temperatures in the western Pacific warm pool over the past 1.75 million years. *Nature*, *433*(7023), 294–298. https://doi.org/10.1038/nature03189

Dekens, P. S., Ravelo, A. C., & McCarthy, M. D. (2007). Warm upwelling regions in the Pliocene warm period. *Paleoceanography*, *22*(3), PA3211. https://doi.org/10.1029/2006pa001394

Donohoe, A., Atwood, A. R., & Battisti, D. S. (2022). Optimal geometric characterization of forced zonal mean tropical precipitation changes. *Climate Dynamics*, *59*(7–8), 2181–2196. https://doi.org/10.1007/s00382-022-06203-6

Dyez, K. A., & Ravelo, A. C. (2013). Late Pleistocene tropical Pacific temperature sensitivity to radiative greenhouse gas forcing. *Geology*, *41*(1), 23–26. https://doi.org/10.1130/g33425.1

Dyez, K. A., & Ravelo, A. C. (2014). Dynamical changes in the tropical Pacific warm pool and zonal SST gradient during the Pleistocene. *Geophysical Research Letters*, *41*(21), 7626–7633. https://doi.org/10.1002/2014gl061639

Etourneau, J., Schneider, R., Blanz, T., & Martinez, P. (2010). Intensification of the Walker and Hadley atmospheric circulations during the Pliocene–Pleistocene climate transition. *Earth and Planetary Science Letters*, *297*(1–2), 103–110. https://doi.org/10.1016/j.epsl.2010.06.010

Fedorov, A. V., Burls, N. J., Lawrence, K. T., & Peterson, L. C. (2015). Tightly linked zonal and meridional sea surface temperature gradients over the past five million years. *Nature Geoscience*, *8*(12), 975–980. https://doi.org/10.1038/ngeo2577

Ford, H. L., Ravelo, A. C., Dekens, P. S., LaRiviere, J. P., & Wara, M. W. (2015). The evolution of the equatorial thermocline and the early Pliocene El Padre mean state. *Geophysical Research Letters*, *42*(12), 4878–4887. https://doi.org/10.1002/2015gl064215

Haug, G. H., Sigman, D. M., Tiedemann, R., Pedersen, T. F., & Sarnthein, M. (1999). Onset of permanent stratification in the subarctic Pacific Ocean. *Nature*, *401*(6755), 779–782. https://doi.org/10.1038/44550

Herbert, T. D., Peterson, L. C., Lawrence, K. T., & Liu, Z. (2010). Tropical ocean temperatures over the past 3.5 million years. *Science*, *328*(5985), 1530–1534. https://doi.org/10.1126/science.1185435

Holloway, M. D., Sime, L. C., Singarayer, J. S., Tindall, J. C., & Valdes, P. J. (2016). Reconstructing paleosalinity from δ18O: Coupled model simulations of the Last Glacial Maximum, Last Interglacial and Late Holocene. *Quaternary Science Reviews*, *131*, 350–364. https://doi.org/10.1016/j.quascirev.2015.07.007

Hollstein, M., Mohtadi, M., Rosenthal, Y., Moffa Sanchez, P., Oppo, D., Martínez Méndez, G., et al. (2017). Stable oxygen isotopes and Mg/Ca in planktic foraminifera from modern surface sediments of the western Pacific warm pool: Implications for thermocline reconstructions. *Paleoceanography*, *32*(11), 1174–1194. https://doi.org/10.1002/2017pa003122

Jia, G., Chen, F., & Peng, P. a. (2008). Sea surface temperature differences between the western equatorial Pacific and northern South China Sea since the Pliocene and their paleoclimatic implications. *Geophysical Research Letters*, *35*(18), L18609. https://doi.org/10.1029/2008gl034792

Kalnay, E., Kanamitsu, M., Kistler, R., Collins, W., Deaven, D., Gandin, L., et al. (1996). The NCEP/NCAR 40-year reanalysis project. *Bulletin of the American Meteorological Society*, *77*(3), 437–472. https://doi.org/10.1175/1520-0477(1996)077<0437:TNYRP>2.0.CO;2

Kotov, S., & Pälike, H. (2018). *QAnalySeries - a cross-platform time series tuning and analysis tool*. AGU.

LaRiviere, J. P., Ravelo, A. C., Crimmins, A., Dekens, P. S., Ford, H. L., Lyle, M., & Wara, M. W. (2012). Late Miocene decoupling of oceanic warmth and atmospheric carbon dioxide forcing. *Nature*, *486*(7401), 97–100. https://doi.org/10.1038/nature11200

LeGrande, A. N., & Schmidt, G. A. (2011). Water isotopologues as a quantitative paleosalinity proxy. *Paleoceanography*, *26*(3), PA3225. https://doi.org/10.1029/2010pa002043

Lisiecki, L. E., & Raymo, M. E. (2005). A Pliocene-Pleistocene stack of 57 globally distributed benthic δ18O records. *Paleoceanography*, *20*(1), PA1003. https://doi.org/10.1029/2004pa001071

Liu, J., Tian, J., Liu, Z., Herbert, T. D., Fedorov, A. V., & Lyle, M. (2019). Eastern equatorial Pacific cold tongue evolution since the late Miocene linked to extratropical climate. *Science Advances*, *5*(4), eaau6060. https://doi.org/10.1126/sciadv.aau6060

Liu, W., Liu, Z., Sun, J., Song, C., Chang, H., Wang, H., et al. (2020). Onset of permanent Taklimakan Desert linked to the mid-Pleistocene transition. *Geology*, *48*(8), 782–786. https://doi.org/10.1130/g47406.1

Liu, Z., Cleaveland, L. C., & Herbert, T. D. (2008). Early onset and origin of 100-kyr cycles in Pleistocene tropical SST records. *Earth and Planetary Science Letters*, *265*(3–4), 703–715. https://doi.org/10.1016/j.epsl.2007.11.016

Locarnini, R. A., Mishonov, A. V., Antonov, J. I., Boyer, T. P., Garcia, H. E., Baranova, O. K., et al. (2013). In S. Levitus (Ed.), *World Ocean Atlas 2013, volume 1: Temperature*, *NOAA Atlas NESDIS* (p. 40).

McClymont, E. L., Elmore, A. C., Kender, S., Leng, M. J., Greaves, M., & Elderfield, H. (2016). Pliocene-Pleistocene evolution of sea surface and intermediate water temperatures from the southwest Pacific. *Paleoceanography*, *31*(6), 895–913. https://doi.org/10.1002/2016PA002954

McClymont, E. L., & Rosell-Melé, A. (2005). Links between the onset of modern Walker circulation and the mid-Pleistocene climate transition. *Geology*, *33*(5), 389–392. https://doi.org/10.1130/g21292.1

McClymont, E. L., Sosdian, S. M., Rosell-Melé, A., & Rosenthal, Y. (2013). Pleistocene sea-surface temperature evolution: Early cooling, delayed glacial intensification, and implications for the mid-Pleistocene climate transition. *Earth-Science Reviews*, *123*, 173–193. https://doi.org/10.1016/j.earscirev.2013.04.006

McGee, D., Donohoe, A., Marshall, J., & Ferreira, D. (2014). Changes in ITCZ location and cross-equatorial heat transport at the Last Glacial Maximum, Heinrich Stadial 1, and the mid-Holocene. *Earth and Planetary Science Letters*, *390*, 69–79. https://doi.org/10.1016/j.epsl.2013.12.043

McGee, D., Moreno-Chamarro, E., Green, B., Marshall, J., Galbraith, E., & Bradtmiller, L. (2018). Hemispherically asymmetric trade wind changes as signatures of past ITCZ shifts. *Quaternary Science Reviews*, *180*, 214–228. https://doi.org/10.1016/j.quascirev.2017.11.020

Medina-Elizalde, M., & Lea, D. W. (2005). The mid-Pleistocene transition in the tropical Pacific. *Science*, *310*(5750), 1009–1012. https://doi.org/10.1126/science.1115933

Meng, X., Liu, L., Wang, X. T., Balsam, W., Chen, J., & Ji, J. (2018). Mineralogical evidence of reduced East Asian summer monsoon rainfall on the Chinese loess plateau during the early Pleistocene interglacials. *Earth and Planetary Science Letters*, *486*, 61–69. https://doi.org/10.1016/j.epsl.2017.12.048

Mohtadi, M., Prange, M., Oppo, D. W., De Pol-Holz, R., Merkel, U., Zhang, X., et al. (2014). North Atlantic forcing of tropical Indian Ocean climate. *Nature*, *509*(7498), 76–80. https://doi.org/10.1038/nature13196

Peng, N., Dang, H., Wu, J., Aiello, I. W., & Jian, Z. (2021). Tectonic and climatic controls on the Plio-Pleistocene evolution of sediment discharge from Papua New Guinea. *Marine Geology*, *441*, 106627. https://doi.org/10.1016/j.margeo.2021.106627

Peterson, L. C., Lawrence, K. T., Herbert, T. D., Caballero-Gill, R., Wilson, J., Huska, K., et al. (2020). Plio-Pleistocene hemispheric (a)symmetries in the northern and southern hemisphere midlatitudes. *Paleoceanography and Paleoclimatology*, *35*(3), e2019PA00372. https://doi.org/10.1029/2019pa003720

Pontes, G. M., Taschetto, A. S., Sen Gupta, A., Santoso, A., Wainer, I., Haywood, A. M., et al. (2022). Mid-Pliocene El Niño/Southern Oscillation suppressed by Pacific intertropical convergence zone shift. *Nature Geoscience*, *15*(9), 726–734. https://doi.org/10.1038/s41561-022-00999-y

Raddatz, J., Nürnberg, D., Tiedemann, R., & Rippert, N. (2017). Southeastern marginal West Pacific Warm Pool sea-surface and thermocline dynamics during the Pleistocene (2.5–0.5 Ma). *Palaeogeography, Palaeoclimatology, Palaeoecology*, *471*, 144–156. https://doi.org/10.1016/j.palaeo.2017.01.024

Russon, T., Elliot, M., Sadekov, A., Cabioch, G., Corrège, T., & De Deckker, P. (2010). Inter-hemispheric asymmetry in the early Pleistocene Pacific warm pool. *Geophysical Research Letters*, *37*(11), L11601. https://doi.org/10.1029/2010gl043191

Russon, T., Elliot, M., Sadekov, A., Cabioch, G., Corrège, T., & De Deckker, P. (2011). The mid-Pleistocene transition in the subtropical southwest Pacific. *Paleoceanography*, *26*(1), PA1211. https://doi.org/10.1029/2010pa002019

Sachs, J. P., Sachse, D., Smittenberg, R. H., Zhang, Z., Battisti, D. S., & Golubic, S. (2009). Southward movement of the Pacific intertropical convergence zone AD 1400–1850. *Nature Geoscience*, *2*(7), 519–525. https://doi.org/10.1038/ngeo554

Schlitzer, R. (2015). Ocean data view. Retrieved from https://odv.awi.de/

Schmidt, M. W., & Spero, H. J. (2011). Meridional shifts in the marine ITCZ and the tropical hydrologic cycle over the last three glacial cycles. *Paleoceanography*, *26*(1), PA1206. https://doi.org/10.1029/2010pa001976

Schneider, T., Bischoff, T., & Haug, G. H. (2014). Migrations and dynamics of the intertropical convergence zone. *Nature*, *513*(7516), 45–53. https://doi.org/10.1038/nature13636

Seo, I., Lee, Y. I., Kim, W., Yoo, C. M., & Hyeong, K. (2015). Movement of the Intertropical Convergence Zone during the mid-pleistocene transition and the response of atmospheric and surface ocean circulations in the central equatorial Pacific. *Geochemistry, Geophysics, Geosystems*, *16*(11), 3973–3981. https://doi.org/10.1002/2015gc006077

Shipboard Scientific Party. (1993). Site 871. In I. Premoli Silva, J. Haggerty, & F. Rack(Eds.), *Proceedings of the Ocean Drilling Program, initial reports* (Vol. 144, pp. 105–144). Ocean Drilling Program.

Stott, L., Poulsen, C., Lund, S., & Thunell, R. (2002). Super ENSO and global climate oscillations at millennial time scales. *Science*, *297*(5579), 222–226. https://doi.org/10.1126/science.1071627

Sun, H., Li, T., Liu, C., Chang, F., Sun, R., Xiong, Z., & An, B. (2017). Variations in the western Pacific warm pool across the mid-Pleistocene: Evidence from oxygen isotopes and coccoliths in the West Philippine Sea. *Palaeogeography, Palaeoclimatology, Palaeoecology*, *483*, 157–171. https://doi.org/10.1016/j.palaeo.2017.07.008

Taylor, S. P., Patterson, M. O., Lam, A. R., Jones, H., Woodard, S. C., Habicht, M. H., et al. (2022). Expanded North Pacific subtropical gyre and heterodyne expression during the mid-Pleistocene. *Paleoceanography and Paleoclimatology*, *37*(5), e2021PA004395. https://doi.org/10.1029/2021pa004395

Wang, X., Wang, Y., Dyez, K. A., Ravelo, A. C., Sun, C. X., Liu, F., et al. (2023). Dataset for paper "Southward shift and intensification of the intertropical convergence zone in the North Pacific across the mid-Pleistocene transition" submitted to Geophysical Research Letters [Dataset]. Zenodo. https://doi.org/10.5281/zenodo.10158618

Wara, M. W., Ravelo, A. C., & Delaney, M. L. (2005). Permanent El Niño-like conditions during the Pliocene warm period. *Science*, *309*(5735), 758–761. https://doi.org/10.1126/science.1112596

Yan, H., Wei, W., Soon, W., An, Z., Zhou, W., Liu, Z., et al. (2015). Dynamics of the intertropical convergence zone over the western Pacific during the Little Ice Age. *Nature Geoscience*, *8*(4), 315–320. https://doi.org/10.1038/ngeo2375

Yan, X.-H., Ho, C.-R., Zheng, Q., & Klemas, V. (1992). Temperature and size variabilities of the Western Pacific Warm Pool. *Science*, *258*(5088), 1643–1645. https://doi.org/10.1126/science.258.5088.1643

Zeng, L., Yi, S., Zhang, W., Feng, H., Lv, A., Zhao, W., et al. (2020). Provenance of loess deposits and stepwise expansion of the desert environment in NE China since ~1.2 Ma: Evidence from Nd-Sr isotopic composition and grain-size record. *Global and Planetary Change*, *185*, 103087. https://doi.org/10.1016/j.gloplacha.2019.103087

Zhan, T., Yang, Y., Liang, Y., Liu, X., Zeng, F., Ge, J., et al. (2023). Decreasing summer monsoon precipitation during the Mid-Pleistocene transition revealed by a pollen record from lacustrine deposits of the Northeast Plain of China. *Palaeogeography, Palaeoclimatology, Palaeoecology*, *611*, 111357. https://doi.org/10.1016/j.palaeo.2022.111357

Zhang, P., Xu, J., Holbourn, A., Kuhnt, W., Xiong, Z., & Li, T. (2022). Obliquity induced latitudinal migration of the intertropical convergence zone during the past ~410 kyr. *Geophysical Research Letters*, *49*(21), e2022GL100039. https://doi.org/10.1029/2022gl100039

Zhao, D., Wan, S., Lu, Z., Zhai, L., Feng, X., Shi, X., & Li, A. (2020). Response of heterogeneous rainfall variability in East Asia to Hadley circulation reorganization during the late Quaternary. *Quaternary Science Reviews*, *247*, 106562. https://doi.org/10.1016/j.quascirev.2020.106562

Zhong, Y., Shi, X., Yang, H., Wilson, D. J., Hein, J. R., Kaboth-Bahr, S., et al. (2022). Humidification of Central Asia and equatorward shifts of westerly winds since the late Pliocene. *Communications Earth & Environment*, *3*(1), 274. https://doi.org/10.1038/s43247-022-00604-5

Zweng, M. M., Reagan, J. R., Antonov, J. I., Locarnini, R. A., Mishonov, A. V., Boyer, T. P., et al. (2013). In S. Levitus (Ed.), *World Ocean Atlas 2013, volume 2: Salinity* (p. 39). NOAA Atlas NESDIS.

References From the Supporting Information

Adler, R., Sapiano, M., Huffman, G., Wang, J.-J., Gu, G., Bolvin, D., et al. (2018). The global precipitation climatology project (GPCP) monthly analysis (new version 2.3) and a review of 2017 global precipitation. *Atmosphere*, *9*(4), 138. https://doi.org/10.3390/atmos9040138

Mudelsee, M. (2000). Ramp function regression: A tool for quantifying climate transitions. *Computers & Geosciences*, *26*(3), 293–307. https://doi.org/10.1016/S0098-3004(99)00141-7

Westerhold, T., Marwan, N., Drury, A. J., Liebrand, D., Agnini, C., Anagnostou, E., et al. (2020). An astronomically dated record of Earth's climate and its predictability over the last 66 million years. *Science*, *369*(6509), 1383–1387. https://doi.org/10.1126/science.aba6853